Batteries & Supercaps

Research Article
doi.org/10.1002/batt.202300003

Chemistry Europe
European Chemical Societies Publishing

www.batteries-supercaps.org

(Localized) Highly Concentrated Electrolytes for Calcium Batteries

Pierre-Alexandre Martin,[a, b] Fabian Årén,[a, c] and Patrik Johansson*[a, c, d]

The concept of non-aqueous highly concentrated electrolytes (HCEs) for modern rechargeable batteries has recently evolved further by also adding a non-coordinating solvent, i.e., a diluent, to create localized HCEs (LHCEs). LHCEs rely on a charge carrier design similar to that of HCEs in synergy with tailored macroscopic properties, especially reduced viscosity. LHCEs have now been extensively investigated for monovalent Li^+ and Na^+ based batteries, but here we investigate both HCEs and LHCEs for divalent Ca^{2+} conducting systems. Here we systematically map both molecular and macroscopic features as function of composition of $Ca(TFSI)_2$ (calcium bis(trifluoromethane)sulfonimide) in PC (propylene carbonate) based HCEs as well as the corresponding LHCEs created using TTE (1,1,2,2-tetrafluoroethyl-2,2,3,3-tetrafluoropropyl ether) as diluent. Some unique HCE properties arise already at ca. 2.00 m, which is at a lower salt concentration than for monovalent systems, and in addition the local structure of the HCE can be maintained even within a nominal 0.45 m LHCE (starting from a 3.26 m parent HCE). The combined observations made at molecular and macro levels pave the way for further optimization of important physico-chemical properties, proper design of electrochemical investigations, and eventually a better understanding of how to best improve the desolvation kinetics at e.g., the electrolyte/electrode interfaces of a Ca metal anode.

Introduction

Sustainable and affordable energy for all, as for instance outlined in United Nation's Sustainable Development Goal #7,[1] implies better ways to store renewable energy generated from e.g., solar and wind power. Today there is fast progress in the area of large-scale electrochemical energy storage (EES) and foremost lithium-ion batteries (LIBs) are utilized at MW-GW scale and moving towards GW-TW scale.[2] There are, however, concerns of long-term sustainability and large price fluctuations of the elements and materials used in LIBs, foremost cobalt (Co) and nickel (Ni) used in NMC and NCA cathodes. For LIBs based on $LiFePO_4$ cathodes, lithium itself as well as natural graphite are still problematic. This has been recognized by the battery R&D community, which pushes for various next generation battery (NGB) technologies in a very agnostic fashion for EES.[3,4]

Within the portfolio of NGBs, multivalent batteries, based on Zn^{2+}, Mg^{2+}, Ca^{2+}, and Al^{3+}, are a fundamentally very promising multifaceted family, both with respect to various performance related measures and from a sustainability perspective.[5–7] Very recently calcium batteries (CaBs) have been highlighted as an especially interesting option as: *i*) Ca itself is the 5th most abundant element in the Earth's crust, and thus holds promise for long term sustainability, *ii*) Ca has a low standard reduction potential of −2.87 V vs. SHE i.e., close to that of Li (−3.04 V), thus promise of creating high-voltage cells – in stark difference to Mg (−2.38 V) and especially to Al (−1.66 V) and Zn (−0.76 V) based batteries, and *iii*) Ca^{2+} is less polarizing, and should therefore exhibit faster kinetics than both Mg^{2+} and Al^{3+}.[8,9] CaBs based on calcium metal anodes hold promise of high both volumetric and gravimetric energy densities as shown by "real" cell level simulations:[10] up to ca. 400 Wh/kg and 1000 Wh/L when using an (imaginary) 200 mAh/g capacity cathode and a rather modest cell voltage of 3.5 V.

Yet, however, in reality operation of CaBs is at best sluggish, with low C-rates and elevated temperature needed.[9] Much of this originates in the electrolytes used and foremost the slow kinetics at the electrolyte/electrode interfaces. For instance, the seminal work by Ponrouch et al. used both a "low" salt concentration electrolyte, 0.45 M $Ca(BF_4)_2$ in standard carbonate solvents, and an elevated temperature, 100 °C, to achieve reversible electroplating.[11] Many similar electrochemical studies have followed using also other Ca-salts,[12–18] some with very non-standard weakly coordinating anions (WCAs),[16–20] but no silver bullet electrolyte has emerged. In parallel, there has been both experimental and computational efforts made to connect

[a] Dr. P.-A. Martin, F. Årén, Prof. P. Johansson
Department of Physics
Chalmers University of Technology
412 96 Gothenburg (Sweden)
E-mail: patrik.johansson@chalmers.se
[b] Dr. P.-A. Martin
Solvionic SA
11 Chemin des Silos, 31100 Toulouse (France)
[c] F. Årén, Prof. P. Johansson
Compular AB
Vasagatan 5B, 411 24 Gothenburg (Sweden)
[d] Prof. P. Johansson
ALISTORE-European Research Institute
CNRS FR 3104, Hub de l'Energie
Rue Baudelocque, 80039 Amiens (France)

Supporting information for this article is available on the WWW under https://doi.org/10.1002/batt.202300003

An invited contribution to a Special Collection dedicated to NordBatt 2022 conference

Research Article
doi.org/10.1002/batt.202300003
Chemistry Europe
European Chemical Societies Publishing

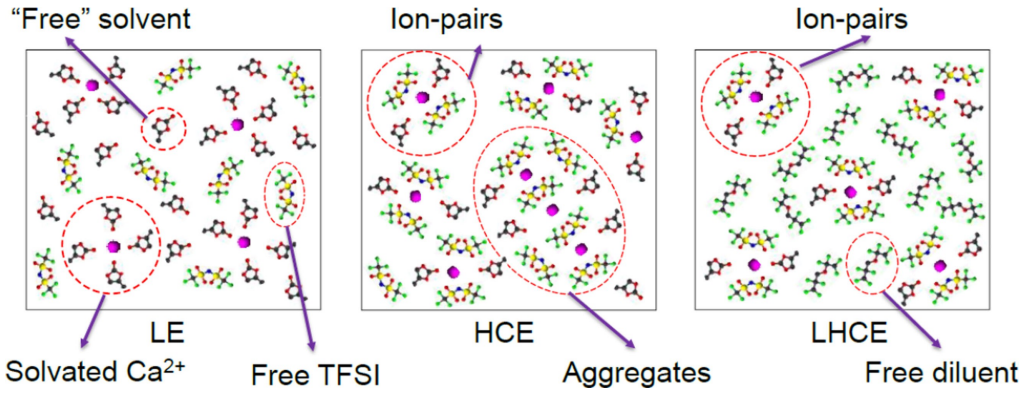

Scheme 1. The conceptual differences between LEs, HCEs, and LHCEs for $Ca(TFSI)_2$ as salt. Inspired by Ref. [32].

the molecular level interactions to the observed physico-chemical properties as well as to practical CaB performance.[21–23]

All the above studies used more[21,22] or less[14,23] standard "salt-in-solvent" liquid electrolytes (LEs). In stark contrast both Li^+ and Na^+ based batteries have seen an increased interest in applying *conceptually* different electrolytes, such as highly concentrated electrolytes (HCEs), also known as "solvent-in-salt" electrolytes[24–28] offering wider electrochemical stability windows (ESWs), reduced volatilities, and increased liquidus ranges. This is either directly or indirectly related to the electrolyte speciation, moving from being rich in "free" (non-coordinated) solvent and well-separated ions as charge carriers in LEs, to less free solvent and more extensive ion-pairing in HCEs (Scheme 1, left and middle). Some HCEs finally create ionic (percolating) networks with little or no free solvent.[28] This is also concomitant with changed coordination and solvation numbers (CNs and SNs) and modes of (cat)ion transport.[29–31] The creation of cation first solvation shells rich in anions and few/no "free" solvent molecules is beneficial for physical-chemical-electrochemical stability – and possibly also for ion transfer at the electrolyte/electrode interface, but it also results in rather poor ionic conductivities and high viscosities.[24–31] This causes both severe mass transport limitations as well as poor wettability of electrodes and separators. In addition, the electrolyte cost can be expected to be more or less proportional to the concentration of the most often rather expensive salt.

In order to tackle these challenges, the concept of localized HCEs (LHCEs) was launched.[32–34] The idea of LHCEs is basically to keep the local properties such as the charge carrier species of HCEs but alter the macroscopic dynamic electrolyte properties. This is accomplished by introducing a non-coordinating solvent, i.e., a diluent (Scheme 1, right). All other matters aside, this should also, even for relatively expensive diluents, lower the electrolyte cost. The diluents are often heavily fluorinated ethers, such as bis(2,2,2-trifluoroethyl) ether (BTFE) and 1,1,2,2-tetrafluoroethyl 2,2,3,3-tetrafluoropropyl ether (TTE),[32] offering a combination of low permittivity and low donor number (DN), while arguably both their cost and sustainability are questionable.

To the best of our knowledge neither HCEs nor LHCEs have previously been reported as CaB non-aqueous electrolytes, excepted the 1.5 M calcium bis(trifluoromethanesulfonyl)imide ($Ca(TFSI)_2$) in various carbonate solvents electrolytes reported on by one of us only very briefly.[21] Herein, we in detail and systematically map both the local physico-chemical and the global macroscopic properties for a wide range of HCEs and LHCEs, based on $Ca(TFSI)_2$ dissolved in propylene carbonate (PC) as solvent and with TTE as diluent.

Experimental and Computational

Materials and electrolyte preparation

All HCEs were prepared by direct mixing of stoichiometric amounts of the salt ($Ca(TFSI)_2$, Solvionic, 99.5%), and the solvent (PC, Aldrich, anhydrous, 99.7%) by stirring overnight on a hotplate at 50 °C. In total 9 different HCEs were prepared and the maximum salt concentration obtained was 3.26 m, which corresponds to a 1:3 Ca:PC molar ratio. All HCEs are to be found on the left side of the ternary composition diagram (Figure 1).

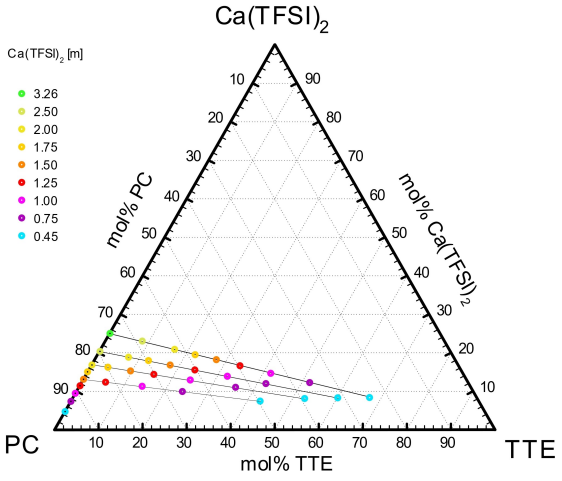

Figure 1. Ternary composition diagram of the HCEs and the LHCEs.

All LHCEs were prepared similarly, with the addition of the diluent (TTE, Apollo scientific, 99%). (The alternative procedure of first preparing the HCE and then adding the diluent did not result in any notable differences as determined by Raman spectroscopy). Four sets of LHCEs were made, summing up to in total 25 electrolytes, each represented by a sloping line left-to-right in the ternary composition diagram: *i*) 8 in the range 0.45–2.50 m, starting from the 3.26 m HCE composition, *ii*) 7 in the range 0.45–2.00 m from the 2.50 m HCE, *iii*) 6 in the range 0.45–1.75 m from the 2.00 m HCE, and *iv*) 4 in the range 0.45–1.25 m from the 1.50 m HCE. All materials and electrolytes were prepared in an Ar filled glove-box (<1 ppm O_2, <1 ppm H_2O) and kept therein until characterization. The water content was <100 ppm for all salts, solvents and electrolytes as measured by Karl-Fisher coulometry (Metrohm 831 Coulometer).

Physico-chemical characterization

The ionic conductivities were measured from 20 to 70 °C in 10 °C steps, with an equilibration time of 20 min at each temperature, by broadband dielectric spectroscopy using a Novocontrol Concept 80 equipment. The DC conductivities were extracted from the AC high frequency plateaus. Coin-cells with stainless steel (SS) electrodes were filled with 100 μL of electrolyte in controlled atmosphere, using a PTFE spacer with a 5 mm inner ring diameter and a thickness of 1 mm. Three coin-cells were prepared for each of the electrolytes to assure repeatability.

The densities and the viscosities (Table S1) were likewise measured from 20 to 70 °C in 10 °C steps, using an Anton Paar DMA 4500 M density meter equipped with a Lovis 2000 M rolling ball viscometer module.

Raman spectra were acquired at room-temperature using a Bruker MultiRAM FT-Raman spectrometer for 1000 scans with a spectral resolution of 2 cm^{-1} using a Nd:YAG laser (1064 nm, 500 mW) as the excitation source. Fitting and deconvolution of the spectra were performed in selected regions to address the TFSI and PC speciation separately using the PeakFit™ software and Voigt functions.

Density functional theory (DFT) calculations

To assist in a semi-quantitative analysis of the speciation via interpretation of the Raman spectra, a few simple DFT calculations were performed using the B3LYP and M06-2X functionals and the 6–311G(d,p) basis set, employing an implicit solvent (water) via the PCM/SCRF methodology.[35,36] For the most stable geometries obtained for the "free" TFSI anion, Ca^{2+}-TFSI ion-pairs and neutral triplets,[22] pure PC, and $[Ca(PC)_x]^{2+}$ ($x=1$–8) solvates (created similarly as in Ref. [22], but replacing DMF by PC), the vibrational frequencies and the corresponding Raman activities were calculated analytically by 2nd and partial 3rd derivatives of the energy, respectively (Table S2). Furthermore, the geometries/molecular structures, total energies, and binding energies for the main species are to be found in Table S3. For this first approximation and semi-quantitative analysis no mixed cation-anion-solvent systems were used. All calculations were made using the Gaussian16 software[37] and starting geometries created in Avogadro.[38] The log-files for the DFT calculations are available upon reasonable request.

Results and Discussions

First a comparison between the LEs and HCEs is made by monitoring basic physico-chemical properties as function of salt concentration. Subsequently these are correlated with the speciation changes, as derived from the Raman spectroscopy analysis leveraged by DFT calculations. Furthermore, the ionicities of the electrolytes, as obtained from Walden analyses, connects the molecular level local structure origins to the macroscopic level global behaviour. Then, a similar approach is taken for the LHCEs. Finally, some implications and paths forward for practical usage of HCEs and LHCEs for CaB are discussed.

LEs and HCEs

Starting with the ionic conductivity as a function of salt concentration, there is a maximum of ca. 8 mS/cm for the 0.75 m electrolyte at 50 °C (Figure 2), and all data gathered at other temperatures show similar general appearance/trends.

This is in agreement with the literature wherein e.g., $Ca(TFSI)_2$ in EC, PC and DMF show maxima at 0.42–0.57 M at room-temperature and similar ionic conductivities (2–10 mS/cm).[21] Most CaB LEs indeed use a single linear ether solvent, such as DME, at 0.25–0.5 M, due to low salt solubility, or a combination of a linear carbonate, such as DMC or EMC, with EC and/or PC up to 0.8 M.[39–41] Lower salt concentrations both reduce the viscosity and improve the ionic conductivity, emphasizing how the larger charge/radius ratios of divalent cations, such as Mg^{2+} and Ca^{2+}, as compared to Li^+ and Na^+, leads to increased ion-ion[42] and ion-solvent[43] interactions. Notably Mg^{2+} based electrolytes are most often ca. 0.25–0.5 M, even when employing low viscosity solvents such as THF.[7]

Moving to the viscosities these show very simple monotonic and close to linear i.e., Arrhenius temperature dependencies (Figure 3).

The 0.45 m electrolyte is only slightly more viscous than the 0.1 M electrolyte used in the literature,[21] which likely is due to free PC being the dominant species in both. We also find the

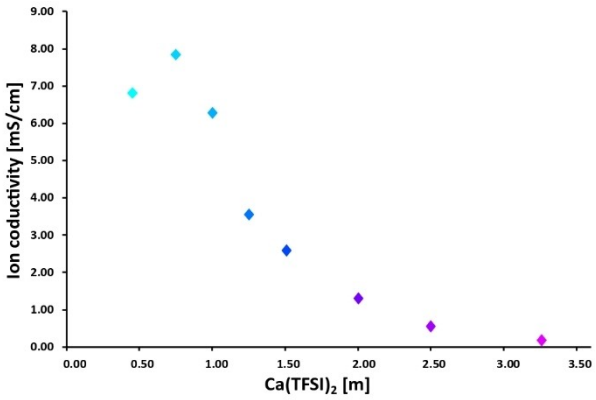

Figure 2. Ionic conductivity as function of salt concentration at 50 °C for the $Ca(TFSI)_2$ in PC electrolytes.

Research Article
doi.org/10.1002/batt.202300003
Chemistry Europe
European Chemical Societies Publishing

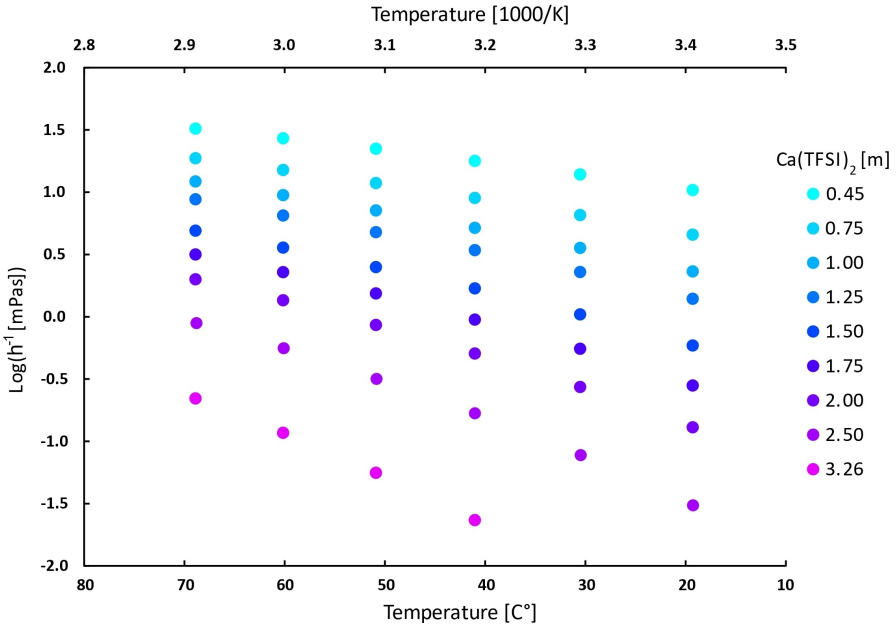

Figure 3. Viscosity as function of temperature and salt concentration for the $Ca(TFSI)_2$ in PC electrolytes. The inverted logarithmic y-axis renders the most viscous/ least fluid electrolytes at the bottom of the graph.

absolute differences between the electrolytes to decrease at elevated temperatures, i.e., their temperature dependencies are somewhat different, and furthermore also to decrease as function of concentration e.g., the 2.00 m and 2.50 m electrolyte data ($\Delta = 0.5$ m) are closer than the 0.45 m and 0.75 m electrolyte data ($\Delta = 0.3$ m). However, the relative salt concentration increases are +25% and +66%, respectively. Finally, there is a clear step function for the 3.26 m electrolyte, having a significantly higher viscosity – more akin to ionic liquid based electrolytes.[44] With its 1:3 Ca:PC molar ratio there is no more enough PC available to create a Ca^{2+} first solvation shell composed only of PC (the preferred partial coordination number (pCN_{PC}) for Ca^{2+} is 5–6, as obtained for the dilute 0.1 M PC electrolyte[21]). Hence, the local structure changes drastically as cation-anion interactions and/or communal solvation becomes increasingly important, as recently observed for Li^+ conducting PC based HCEs.[45] Furthermore, also a percolation network might be formed at these concentrations, affecting both the viscosity, dynamics and the ion transport mechanism.[30,31]

The trends in ionic conductivities and viscosities are for both LEs and HCEs often argued to show how an increased concentration of cation charge carriers is counteracted by the increased viscosity, i.e., slower ion diffusion/migration, and/or increased ion-pairing and aggregation (reducing the number of effective charge carriers) – following a simple Nernst-Einstein equation reasoning. The total ionic conductivity, however, does not provide any information about the relative cation *vs.* anion contributions nor the mode(s) of ion transport, which may differ significantly both as function of salt(s), solvent(s) and salt concentration. A common Walden plot of the (molar) ionic conductivity as function of viscosity, also including temperature effects, provides a phenomenological analysis starting point (Figure 4) .[46]

The interpretation of the Walden plot is complicated due to the mix of divalent cations and monovalent anions.[47] As a sidenote there are other ways to evaluate the contributions of each ion,[48] but Walden plots remain the benchmark tool to evaluate ionicity. That all data are far below the reference line anyhow points to low ionicity i.e., formation of ion-pairs and/or aggregates, and as expected the ionicity decreases as a function of salt concentration. For the <2.00 m electrolytes, both the ionic conductivities and the viscosities have similar temperature dependencies, why all data are quite clustered. When moving to the >2.00 m data, however, there are more notable and clear differences. First, the 2.50 m data have both a slightly different slope, i.e., activation energy, and is found below all the other data. This points to a change in speciation and is qualitatively consistent with that the viscosity is similar to that of the 2.00 m electrolyte (Figure 3) while the ionic conductivity drops by ca. 50% (Figure 2). Second, the much higher viscosity of the 3.26 m electrolyte (Figure 3) is not accompanied by any similar decrease in the ionic conductivity (Figure 2). This points to a decoupling of the ion transport from the limits of viscosity i.e., being non-vehicular. Such a decoupling is one possible route to drastically improved cation transference numbers,[26,30] but the total ionic conductivities are likely prohibitively low. To try to elucidate the connection between these macroscopic properties and the local structure the Ca^{2+} solvation is probed using Raman spectroscopy and a region, 700–760 cm^{-1}, holding information from both PC and TFSI (Figure 5).

The $\gamma_{(C=O)}$ vibrational modes of "free", i.e., non-coordinated, PC at 713 cm^{-1} (circle)[49] and the corresponding Ca^{2+}-coordinated PC at 728 cm^{-1} (grand star) clearly show that moving

Research Article
doi.org/10.1002/batt.202300003
Chemistry Europe
European Chemical Societies Publishing

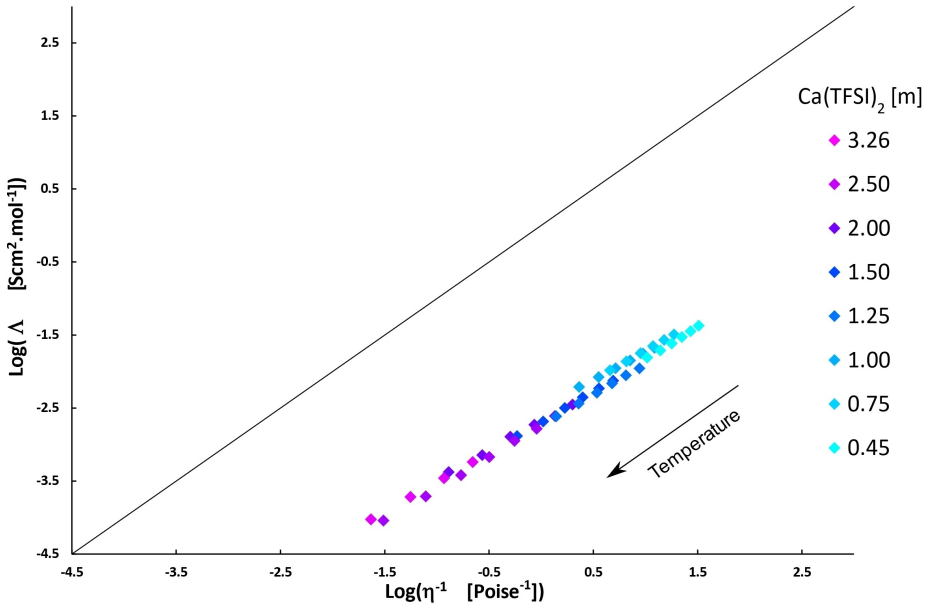

Figure 4. Walden plot for the LEs and HCEs connecting the molar ionic conductivities and viscosities.

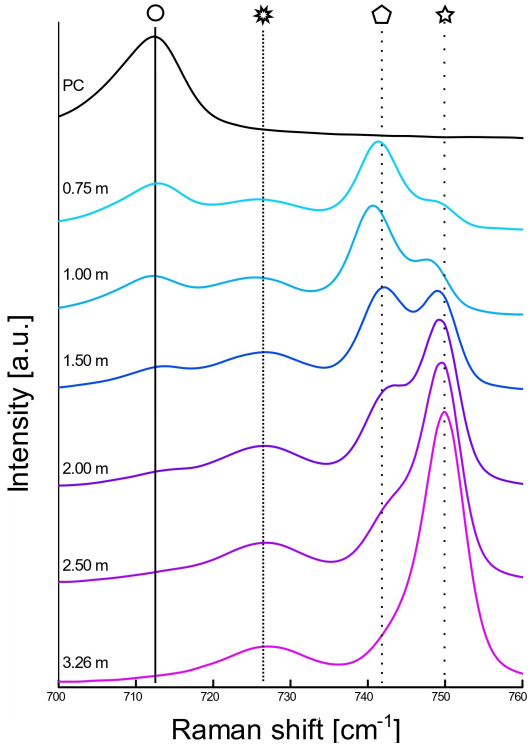

Figure 5. Raman spectra for selected LEs and HCEs in the region sensitive to both cation-anion and cation-solvent interactions: ○"free" PC, ✲ Ca^{2+}-coordinated PC, ⬠ "free" TFSI, and ☆ Ca^{2+}-coordinated TFSI.

from pure PC and LEs (top) towards HCEs (middle and bottom), the former rapidly decreases and concomitantly the Ca^{2+}-PC band increases. For the TFSI breathing mode[50] of "free" TFSI at 741 cm^{-1} (pentagon) and the corresponding Ca^{2+}-coordinated TFSI at 750 cm^{-1} (star)[21] a similar behaviour is observed. Ultimately, for the 3.26 m electrolyte, both the "free" PC and "free" TFSI bands have almost totally disappeared. While the criteria used to define an HCE differs,[24–28] this electrolyte fulfil most/all criteria. A semi-quantitative speciation analysis is made possible by combining the Raman data, fitted and deconvoluted, with the results of the DFT calculations. Figure 6 is an example of a single Raman spectrum fitting showing how the different interactions (cation-solvent and cation-anion) and resulting species are extracted, with all the information obtained from all the Raman spectra summarized in Figure 7.

As the fitting procedure affects the analysis some details are called for; For "free" PC two peaks were used,[49] while for TFSI only a single peak was used for its two conformers as the shift between them is very minor for most ionic systems.[50] The same is true for the coordinated Ca^{2+}-TFSI feature, where we additionally stress that we here do not differentiate between ion-pairs and triplets etc. and solely use triplet DFT data (Table S2). The situation for coordinated PC, however, is much more complex[45] with several possible contributors and therefore no less than three peaks were used (for $x = 4$–6, Table S2) to mimic/represent the differences in the Ca^{2+} CN as function of salt concentration. Overall, this process follows nicely what has been seen and used for both Li, Na and Ca based electrolytes in the literature,[21,45] including differences in CN and speciation. We stress that the DFT calculations show the Raman activities to (very roughly) be proportional to the number of oscillators (Table S2), why the peak areas overall mimic the (relative) populations, even though the CNs of the $[Ca(PC)_x]^{2+}$ complexes change with concentration.

The cross-over concentrations i.e., where more PC solvents and TFSI anions are coordinated than not, are obtained at 0.75 m and 1.50 m, respectively (Figure 7). We note that the

Research Article
doi.org/10.1002/batt.202300003
Chemistry Europe
European Chemical Societies Publishing

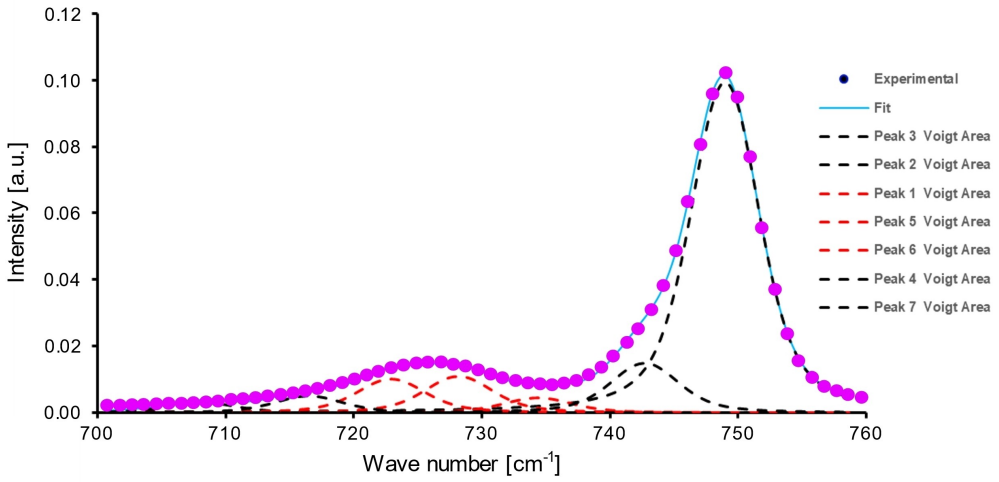

Figure 6. Example of fit and deconvolution performed on the 3.26 m HCE Raman spectra.

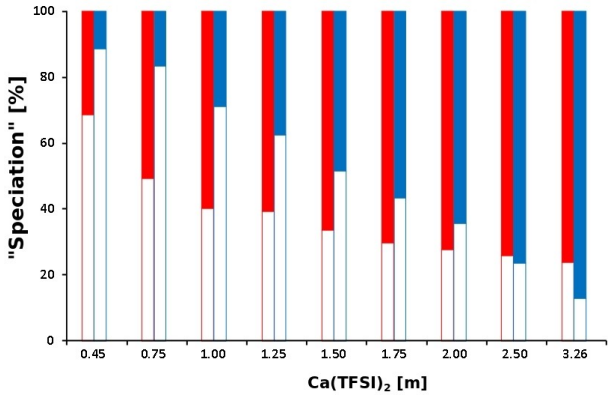

Figure 7. The cation-solvent interactions (red) and the ion-pairing (blue) as function of salt concentration at room temperature for the $Ca(TFSI)_2$ in PC electrolytes. Empty and filled parts correspond to "free" and Ca^{2+}-coordinated species (solvents/anion), respectively.

most conductive electrolyte (0.75 m) (Figure 2), only has 50% "free" PC, but also rather few ion-pairs/triplets (ca. 20%).

The (relative) population of "free" and Ca^{2+}-coordinated PC has an additional caveat of how communal solvation[45] affects the analysis, but from ca. 2.00 m there is only a very slight increase of Ca^{2+}-coordinated PC (Figure 7). From this the 2.00 m electrolyte could be chosen as the first HCE and based on simulations of Li-based systems[30,31] a cationic percolation network could be important, with some 35% of "free" TFSI anions, but neutron scattering studies[52,53] cast a doubt on this to be a general phenomenon. While a cation transference number as high as 0.73(!) has been obtained,[52] this is for an aqueous HCE at much higher (LiTFSI) salt concentrations. In contrast, the same salt in acetonitrile (ACN) at a maximum 2:1 ACN:LiTFSI molar ratio show ligand exchange to contribute only at lower temperatures and the solvation structure to be temperature dependent.[53] For our system, any such changes are also not really supported by the viscosity data (Figure 3); the step change occurs first for the 3.26 m electrolyte.

LHCEs

As stated, to resolve some of the problematic features of HCEs, we can possibly turn to the concept of LHCEs, here created by adding TTE (Figure 1). In order to properly compare between HCEs and LHCEs, "nominal concentration" will henceforth refer to the concentration of $Ca(TFSI)_2$ in the overall electrolyte, including diluent, while "local concentration" refers to the original concentration of the electrolyte, prior to the addition of the diluent. This is indeed the very idea behind the concept of localized HCEs. A direct comparison of the ionic conductivities at the same nominal salt concentrations clearly shows the effect of dilution e.g., at 0.75 m (Figure 8). In contrast, within a LHCE family the dilution does not impact the ionic conductivity to at all the same extent.

Using the local rather than the nominal salt concentrations another picture emerges. Starting from e.g., the 2.00 m HCE, the obtained LHCE data (green) present a maximum at 1.00 m, which is true for all LHCEs, with the highest ionic conductivity being derived from the 1.50 m LE/HCE. That the maximum ionic conductivity appear at approx. 1 m is strikingly similar to traditional monovalent non-aqueous battery electrolytes. Furthermore, for the same nominal concentration, the ionic conductivities are higher the lower the local concentration is, likely due to the charge carrier concentration being less diluted and the global viscosity lower.

The corresponding viscosity data (Table S1) do show a general and large decrease upon addition of TTE and in the Walden plot (Figure 9) all four families of LHCEs move further away from the reference line upon dilution, a behaviour markedly more prominent for the LHCEs starting from the more concentrated HCEs. This reflects that the dilution reduces the ionic conductivity by a similar factor for almost all salt concentrations, while it decreases the viscosity by a larger extent for the more concentrated systems, which in turn we speculate depends on that part of the ion transport is non-vehicular in origin and therefore scale differently.[30]

Research Article
doi.org/10.1002/batt.202300003
Chemistry Europe
European Chemical Societies Publishing

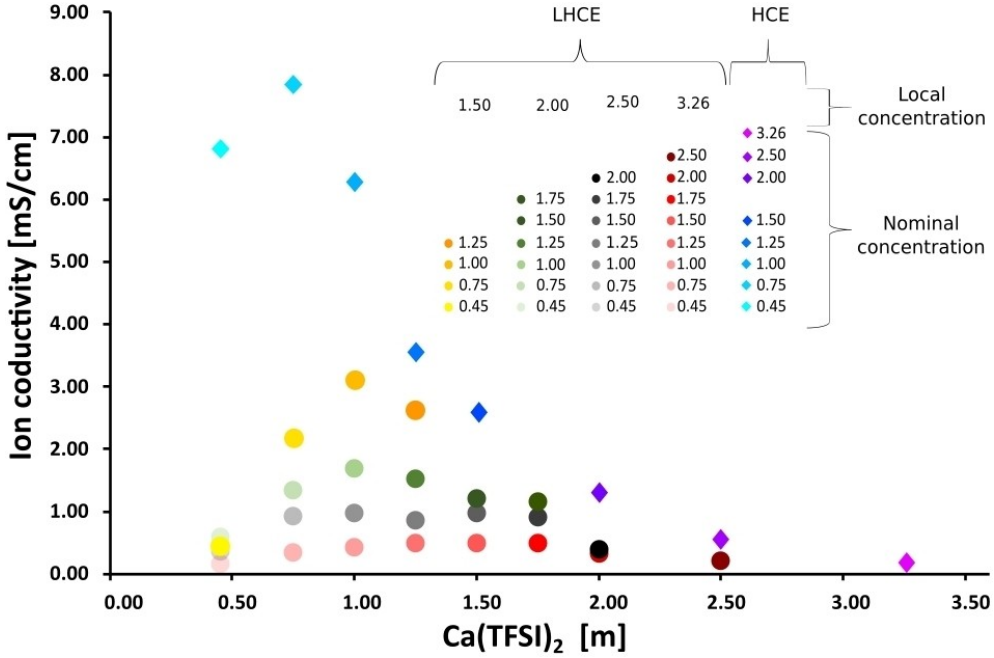

Figure 8. Ionic conductivity as function of salt concentration for the $Ca(TFSI)_2$ in PC and TTE HCEs and LHCEs.

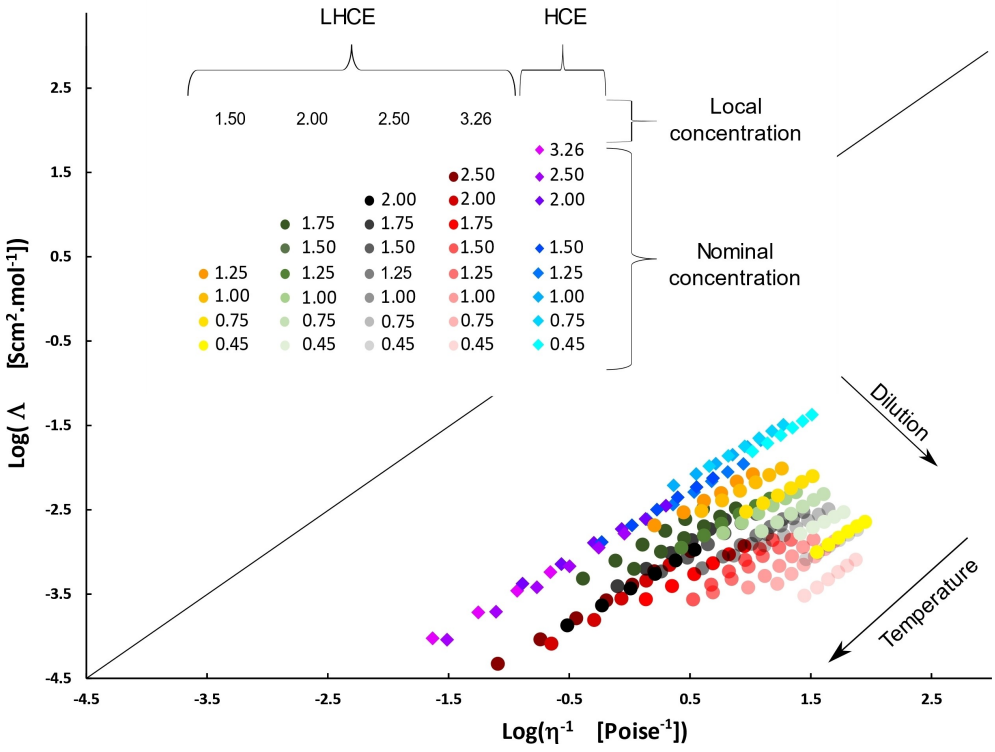

Figure 9. Walden plot for all LEs, HCEs and LHCEs.

Are the prospects for the LHCEs truly accompanied by having a "HCE-like" local structure? From a Raman spectra analysis, performed the same way as for the LEs and HCEs, for neat PC, the 0.45 m LE, the 3.26 m HCE, and the 0.45 m nominal and 3.26 m local concentration LHCE (Figure 10), we find that even after the very large dilution from 3.26 to 0.45 m the Ca^{2+}-PC and Ca^{2+}-TFSI spectral features, i.e., the cation-solvent and ion-pair interactions, do not change significantly and neither do any significant "free" PC or "free" TFSI peaks appear.

Research Article
doi.org/10.1002/batt.202300003
Chemistry Europe
European Chemical Societies Publishing

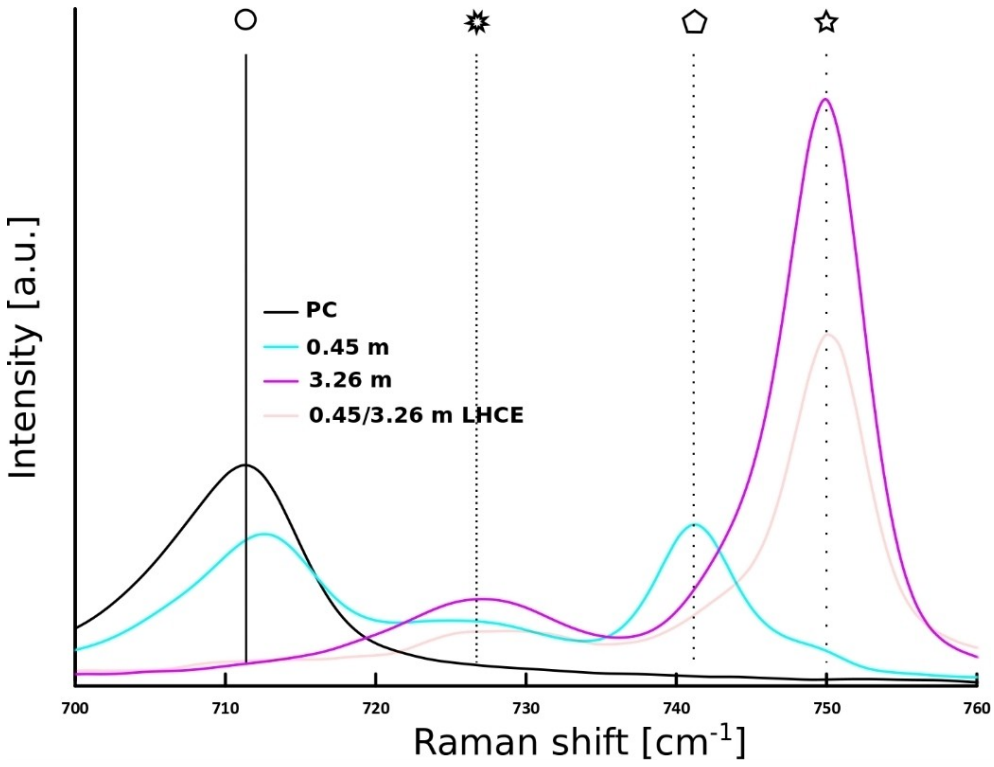

Figure 10. Raman spectra showing the principle of intact local structure of an HCE in an LHCE.

The visually lowered overall Raman intensity of the 0.45/3.26 m LHCE is simply an effect of the reduced number density of these oscillators within the Raman scattering volume, while the overall spectral profile clearly is nowhere close to that of the spectrum of the 0.45 m LE. That the local cation first solvation shell of the parent HCE is conserved is indeed more or less a general feature of the LHCEs and thus calls for some semi-quantitative analysis. Starting with the ion-pairing, the addition of TTE seems to cause minor *increases* in the Ca^{2+}-TFSI interactions (Figure 11).

For the (extreme) case of the 0.75/3.26 m LHCE, a vast 93% of the TFSI anions are found in ion-pairs (or higher aggregates). Furthermore, the (relative) amount of cation-anion interactions is rather freely tailorable e.g., the 0.45/1.50 m LHCE has 68% of ion-pairing, which is more than the 2.00 m HCE has. That the dilution is (relatively) more "efficient" for the nominally less concentrated electrolytes is most likely an effect of the relatively larger concentration of TTE, causing the overall/global permittivity of the electrolyte to drop significantly – which usually triggers ion-pairing.

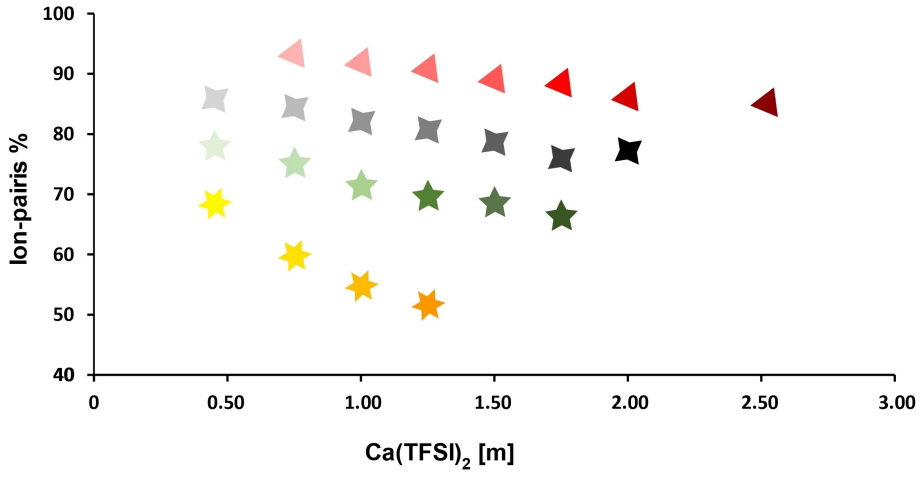

Figure 11. The ion-pairing as function of nominal and local salt concentrations, with the symbols corresponding to the latter: ◀ 3.26 m, ✖ 2.50 m, ★ 2.00 m, and ✶ 1.50 m.

Research Article
doi.org/10.1002/batt.202300003
Chemistry Europe
European Chemical Societies Publishing

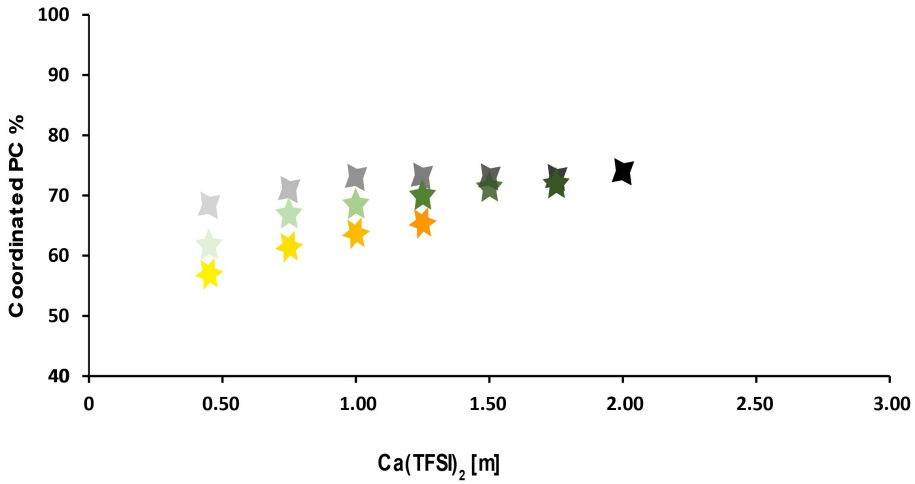

Figure 12. The cation-solvent interactions as function of nominal and local salt concentration, with the symbols corresponding to the latter: ★ 2.50 m, ★ 2.00 m, and ★ 1.50 m.

Turning to the cation-solvent interactions the overall tendency is roughly the reverse with respect to LEs and HCEs, but also much less pronounced (Figure 12). For the local concentration of 3.26 m the Raman spectra signatures for "free" PC were too low in intensity to be unambiguously fitted and were therefore omitted from the analysis.

The relative amount of coordinated PC decreases somewhat upon dilution and becomes lowest for the least concentrated electrolyte, both nominally and locally, the 0.50/1.50 m LHCE, but never goes below 55%. This is to be compared to the cross-over (50%) at 0.75 m for the HCEs (Figure 7). As for the ion-pairing the changes are overall less pronounced for the LHCEs starting from higher nominal salt concentrations, and while it is not unambiguous to directly reveal or quantify the overall "integrity" of the Ca^{2+} first solvation shells even from the combined data of Figures 11 and 12, they do point to that the nominally higher salt concentration used as starting point, the more intact the solvation shells are.

Conclusion

As a very first study of Ca based/conducting HCEs and LHCEs, combining several experimental techniques, we are able to unambiguously show how the macroscopic performance of a wide range of Ca^{2+} electrolytes relate to some specific underlying molecular features and how the trends can be monitored and understood. In the future, it would be intriguing to see how this matches practical CaB cell results. In absolute numbers the 0.75 m electrolyte ionic conductivity could be used as a benchmark and target for other Ca^{2+}-conducting electrolytes based on WCAs and strong permittivity solvents. At the same time, we have in principle only confirmed that HCEs indeed have very high viscosities, but we have also shown that the onset of these properties appear at (much) lower salt concentrations than for monovalent cation based systems. This might be a practical opening for CaB cell creation as well as for the ion transport, especially as the latter can be further decoupled from the viscosity by creating LHCEs.

The integrity of the cation first solvation shell in the LHCEs at the same time as the macroscopic properties are varied is far from easy to directly reveal, but it seems that the higher the nominal salt concentration, the more intact the cation first solvation shell is, and the 0.75/3.26 m LHCE could possibly be used as a benchmark. A caveat is that we do not differentiate between charged (contact) ion-pairs and neutral triplets, and thus neither how these different species may affect the macroscopic properties including the ionic conductivity.

While none of the LHCEs has the ionic conductivity often stated to be needed for practical battery application, the charge carrier nature, may render better cation transfer at the electrolyte/electrode interfaces – an emergent hot topic for multivalent electrolytes.[5,6,23]

Finally, it would be highly advantageous to create LHCEs from non-fluorinated and less expensive diluents as e.g., TTE today comes at ca. 45 $ for 5 g, likely a prohibitively high price.

Acknowledgements

The funding from theEuropean Union's Horizon 2020 research and innovation programme H2020 FETOPEN-1-2016-2017 (CARBAT, grant agreement #766617) is gratefully acknowledged. FÅ and PJ are also grateful for the financial support provided from the Swedish Energy Agency by the project "Highly Concentrated Electrolytes" (#39909-1) within "Batterifondsprogrammet". The continuous support to PJ from several of Chalmers Areas of Advance: Materials Science, Energy, and Transport, is highly appreciated. FÅ and PJ are in addition grateful for the computational resources provided by the Swedish National Infrastructure for Computing (SNIC) at Chalmers Centre for Computational Science and Engineering (C³SE)/e-commons.

Conflict of Interest

The authors declare no conflict of interest.

Data Availability Statement

The data that support the findings of this study are available from the corresponding author upon reasonable request.

Keywords: calcium battery · cation solvation · electrolytes · ion transport · localized highly concentrated electrolytes

[1] https://www.undp.org/sustainable-development-goals.
[2] https://e360.yale.edu/features/in-boost-for-renewables-grid-scale-battery-storage-is-on-the-rise.
[3] A. Z. Weber, M. M. Mench, J. P. Meyers, P. N. Ross, J. T. Gostick, Q. Liu, *J. Appl. Electrochem.* **2011**, *41*, 1137.
[4] H. Kim, D. A. Boysen, J. M. Newhouse, B. L. Spatocco, B. Chung, P. J. Burke, D. J. Bradwell, K. Jiang, A. A. Tomaszowska, K. Wang, W. Wei, L. A. Ortiz, S. A. Barriga, S. M. Poizeau, D. R. Sadoway, *Chem. Rev.* **2013**, *113*, 2075–2099.
[5] Y. Liang, H. Dong, D. Aurbach, Y. Yao, *Nat. Energy* **2020**, *5*, 646–656.
[6] A. Ponrouch, J. Bitenc, R. Dominko, N. Lindahl, P. Johansson, M. R. Palacín, *Energy Storage Mater.* **2019**, *20*, 253–262.
[7] J. Muldoon, C. B. Bucur, T. Gregory, *Chem. Rev.* **2014**, *114*, 11683–11720.
[8] R. J. Gummow, G. Vamvounis, M. B. Kannan, Y. H. He, *Adv. Mater.* **2018**, *30*, 1801702.
[9] M. Arroyo-de Dompablo, A. Ponrouch, P. Johansson, M. R. Palacín, *Chem. Rev.* **2020**, *120*, 6331–6357.
[10] D. Monti, A. Ponrouch, R. Barros, F. Barde, P. Johansson, M. R. Palacín, *Front. Chem.* **2019**, *7*, 79.
[11] A. Ponrouch, C. Frontera, F. Bardé, M. R. Palacín, *Nat. Mater.* **2016**, *15*, 169–172.
[12] Q. Wei, L. Zhang, X. Sun, T. L. Liu, *Chem. Sci.* **2022**, *13*, 5797.
[13] N. T. Hahn, S. A. McClary, A. T. Landers, K. R. Zavadil, *J. Phys. Chem. C* **2022**, *126*, 10335–10345.
[14] N. T. Hahn, J. Self, D. M. Driscoll, N. Dandu, K. Sung Han, V. Murugesan, K. T. Mueller, L. A. Curtiss, M. Balasubramanian, K. A. Persson, K. R. Zavadil, *Phys. Chem. Chem. Phys.* **2022**, *24*, 674.
[15] D. Wang, X. Gao, Y. Chen, L. Jin, C. Kuss, P. G. Bruce, *Nat. Mater.* **2018**, *17*, 16–20.
[16] A. Shyamsunder, L. E. Blanc, A. Assoud, L. F. Nazar, *ACS Energy Lett.* **2019**, *4*, 2271–2276.
[17] Z. Li, O. Fuhr, M. Fichtner, Z. Zhao-Karger, *Energy Environ. Sci.* **2019**, *12*, 3496–3501.
[18] J. Bitenc, A. Scafuri, K. Pirnat, M. Lozinšek, I. Jerman, J. Grdadolnik, B. Fraisse, R. Berthelot, L. Stievano, R. Dominko, *Batteries & Supercaps* **2021**, *4*, 214–220.
[19] N. J. Leon, X. Xie, M. Yang, D. M. Driscoll, J. G. Connell, S. Kim, T. Seguin, J. T. Vaughey, M. Balasubramanian, K. A. Persson, C. Liao, *J. Phys. Chem. C* **2022**, *126*, 13579–13584.
[20] S. H. Strauss, *Chem. Rev.* **1993**, *93*, 927–942.
[21] J. D. Forero-Saboya, E. Marchante, R. B. Araujo, D. Monti, P. Johansson, A. Ponrouch, *J. Phys. Chem. C* **2019**, *123*, 29524–29532.
[22] R. B. Araújo, V. Thangavel, P. Johansson, *Energy Storage Mater.* **2021**, *39*, 89–95.
[23] S. Hou, X. Ji, K. Gaskell, P. Wang, L. Wang, J. Xu, R. Sun, O. Borodin, C. Wang, *Science* **2021**, *374*, 172–178.
[24] Y. Yamada, M. Yaegashi, T. Abe, A. Yamada, *Chem. Commun.* **2013**, *49*, 11194–11196.
[25] D. M. Seo, O. Borodin, S.-D. Han, P. D. Boyle, W. A. Henderson, *J. Electrochem. Soc.* **2012**, *159*, A1489–A1500.
[26] L. Suo, Y.-S. Hu, H. Li, M. Armand, L. Chen, *Nat. Commun.* **2013**, *4*, 1481.
[27] O. Borodin, J. Self, K. A. Persson, C. Wang, K. Xu, *Joule* **2020**, *4*, 69–100.
[28] Y. Yamada, J. Wang, S. Ko, E. Watanabe, A. Yamada, *Nat. Energy* **2019**, *4*, 269–280.
[29] E. Flores, G. Åvall, S. Jeschke, P. Johansson, *Electrochim. Acta* **2017**, *233*, 134–141.
[30] R. Andersson, F. Årén, A. A. Franco, P. Johansson, *J. Electrochem. Soc.* **2020**, *167*, 140537.
[31] C. J. Franko, C.-H. Yim, F. Årén, G. Åvall, P. S. Whitfield, P. Johansson, Y. A. Abu-Lebdeh, G. R. Goward, *J. Electrochem. Soc.* **2020**, *167*, 160532.
[32] X. Cao, H. Jia, W. Xu, J.-G. Zhang, *J. Electrochem. Soc.* **2021**, *168*, 010522.
[33] T. Doi, Y. Shimizu, M. Hashinokuchi, M. Inaba, *J. Electrochem. Soc.* **2017**, *164*, A6412.
[34] J. Zheng, S. Chen, W. Zhao, J. Song, M. H. Engelhard, J.-G. Zhang, *ACS Energy Lett.* **2018**, *3*, 315–321.
[35] E. Cancès, B. Mennucci, J. Tomasi, *J. Chem. Phys.* **1997**, *107*, 3032–3041.
[36] J. Tomasi, B. Mennucci, R. Cammi, *Chem. Rev.* **2005**, *105*, 2999–3094.
[37] Gaussian 16, Revision A.03: M. J. Frisch, G. W. Trucks, H. B. Schlegel, G. E. Scuseria, M. A. Robb, J. R. Cheeseman, G. Scalmani, V. Barone, G. A. Petersson, H. Nakatsuji, X. Li, M. Caricato, A. V. Marenich, J. Bloino, B. G. Janesko, R. Gomperts, B. Mennucci, H. P. Hratchian, J. V. Ortiz, A. F. Izmaylov, J. L. Sonnenberg, D. Williams-Young, F. Ding, F. Lipparini, F. Egidi, J. Goings, B. Peng, A. Petrone, T. Henderson, D. Ranasinghe, V. G. Zakrzewski, J. Gao, N. Rega, G. Zheng, W. Liang, M. Hada, M. Ehara, K. Toyota, R. Fukuda, J. Hasegawa, M. Ishida, T. Nakajima, Y. Honda, O. Kitao, H. Nakai, T. Vreven, K. Throssell, J. A. Montgomery, Jr., J. E. Peralta, F. Ogliaro, M. J. Bearpark, J. J. Heyd, E. N. Brothers, K. N. Kudin, V. N. Staroverov, T. A. Keith, R. Kobayashi, J. Normand, K. Raghavachari, A. P. Rendell, J. C. Burant, S. S. Iyengar, J. Tomasi, M. Cossi, J. M. Millam, M. Klene, C. Adamo, R. Cammi, J. W. Ochterski, R. L. Martin, K. Morokuma, O. Farkas, J. B. Foresman, D. J. Fox, Gaussian, Inc., Wallingford CT, **2016**.
[38] M. D. Hanwell, D. E. Curtis, D. C. Lonie, T. Vandermeersch, E. Zurek, G. R. Hutchison, *J. Cheminf.* **2012**, *4*, 17.
[39] N. Wu, W. Yao, X. Song, G. Zhang, B. Chen, J. Yang, Y. Tang, *Adv. Energy Mater.* **2019**, *9*, 1803865.
[40] M. Wang, C. L. Jiang, S. Q. Zhang, X. H. Song, Y. B. Tang, H. M. Cheng, *Nat. Chem.* **2018**, *10*, 667–672.
[41] S. Wu, F. Zhang, Y. Tang, *Adv. Sci.* **2018**, *5*, 1701082.
[42] D. S. Tchitchekova, D. Monti, P. Johansson, F. Bardé, A. Randon-Vitanova, M. R. Palacín, A. Ponrouch, *J. Electrochem. Soc.* **2017**, *164*, A1384–A1392.
[43] M. Okoshi, Y. Yamada, S. Komaba, A. Yamada, H. Nakai, *J. Electrochem. Soc.* **2017**, *164*, A54–A60.
[44] G. A. Giffin, *J. Mater. Chem. A* **2016**, *4*, 13378–13389.
[45] G. Åvall, J. Wallenstein, G. Cheng, K. Gering, P. Johansson, D. P. Abraham, *J. Electrochem. Soc.* **2021**, *168*, 050521.
[46] P. Walden, *Z. Phys. Chem.* **1906**, *55*, 207–249.
[47] A. Dave, K. L. Gering, J. M. Mitchell, J. Whitacre, V. Viswanathan, *J. Electrochem. Soc.* **2020**, *167*, 013514.
[48] D. Fraenkel, *Chem. Phys. Lett.* **2021**, *781*, 138957.
[49] G. J. Janz, J. Ambrose, J. W. Coutts, J. R. Downey, *Spectrochim. Acta Part A: Mol. Spec.* **1979**, *35*, 175–179.
[50] I. Rey, P. Johansson, J. Lindgren, J.-C. Lassègues, J. Grondin, L. Servant, *J. Phys. Chem. A* **1998**, *102*, 3249–3258.
[51] A. Martinelli, A. Matic, P. Johansson, P. Jacobsson, L. Börjesson, A. Fernicola, S. Panero, B. Scrosati, H. Ohno, *J. Raman Spectrosc.* **2011**, *42*, 522–528.
[52] O. Borodin, L. Suo, M. Gobet, X. Ren, F. Wang, A. Faraone, J. Peng, M. Olguin, M. Schroeder, M. S. Ding, E. Gobrogge, A. von Wald Cresce, S. Munoz, J. A. Dura, S. Greenbaum, C. Wang, K. Xu, *ACS Nano* **2017**, *11*, 10462–10471.
[53] F. Lundin, L. Aguilera, H. Wase Hansen, S. Lages, A. Labrador, K. Niss, B. Frick, A. Matic, *Phys. Chem. Chem. Phys.* **2021**, *23*, 13819–13826.

Manuscript received: January 3, 2023
Revised manuscript received: February 20, 2023
Accepted manuscript online: February 22, 2023
Version of record online: March 8, 2023